IMAGE PROCESSING WITH TRIANGULAR BIORTHOGONAL WAVELETS

Susumu Sakakibara and Oleg V. Vasilyev

School of Information Environment, Tokyo Denki University
2-1200 Muzaigakuendai, Inzai, Chiba, Japan, 270-1382
phone: + (81) 476-46-8748, fax: + (81) 476-46-8499, email: susumu@sie.dendai.ac.jp
web: www.sie.dendai.ac.jp

Department of Mechanical Engineering, University of Colorado
ECME 126, Boulder, Co. 80309-0427
phone: +(1) 303-492-4717, email: Oleg.Vasilyev@colorado.edu

ABSTRACT

We consider new non-separable two dimensional biorthogonal wavelets whose filters are defined on the regular triangular lattice on a plane. Their construction uses lifting in the polyphase representation of the filters, thereby rendering implementation of wavelet transform simple. By applying wavelet transform on actual images, we demonstrate their effectiveness in dealing with images without loosing isotropy.

1. INTRODUCTION

Image processing is one of the major application areas of wavelet transform. It is customary to apply wavelet transform in tensor product form, i.e., one dimensional wavelet transform is applied in horizontal and vertical components of the matrices of image data independently [1]. As a result, isotropy of images may not be well respected. To remedy this drawback, many attempts have been carried out to construct non-separable wavelets [2], or to implement dual-tree wavelet transforms [3, 4]. They are not used as a standard tool, however, because they are not so easy to construct or to use in actual computations.

In the advent of lifting scheme [5], the so-called second generation wavelets [6] have opened a way to handle data on irregular grids over arbitrary surfaces [7]. They seem to gain popularity in efficient parametrization of curved surfaces, in the framework of subdivision scheme [8]. However, isotropy, or rotational symmetry, in two dimensional data is not of major concern.

If we restrict to data on a plane such as images, the usual (first generation) wavelets would be more desirable, since they would allow more general treatments due to their periodicity on the plane. As a first step toward this end, we consider biorthogonal wavelets whose filters are defined on the regular triangular lattice, which we call triangular wavelets. Following the general formalism laid out by one of the authors for orthogonal case [11], we construct simple biorthogonal systems, and study their features that may be relevant in image processing by appying them on actual samples.

After a brief review on biorthogonal wavelets in the next section, we explain how to construct our triangular wavelet filters, in Section 3, by extending the same method as in the usual case. We then apply our triangular biorthogonal filters on actual images, and compare their properties, in Section 4. Suction 5 summarizes our conclusions.

2. BIORTHOGONAL WAVELETS

The discrete signal $\{c_j[k]\}$, $k \in \mathbb{Z}$, is decomposed by the LP filter $\{h[k]\}$ and the HP filter $\{g[k]\}$, followed by downsampling, to yield the coarse componenet $\{c_{j-1}[k]\}$ and detail component $\{d_{j-1}[k]\}$, respectively, of half a resolution. This decomposition is written in terms of the modulation matrix

$$\widehat{M}(\omega) = \begin{pmatrix} \hat{h}(\omega) & \hat{h}(\omega+\pi) \\ \hat{g}(\omega) & \hat{g}(\omega+\pi) \end{pmatrix}$$

as

$$\begin{pmatrix} \hat{c}_{j-1}(2\omega) \\ \hat{d}_{j-1}(2\omega) \end{pmatrix} = \frac{1}{2}\widehat{M}^*(\omega) \begin{pmatrix} \hat{c}_j(\omega) \\ \hat{c}_j(\omega+\pi) \end{pmatrix}, \tag{1}$$

where

$$\hat{c}_j(\omega) = \sum_{k\in\mathbb{Z}} c_j[k]\, e^{-i\omega k}, \quad \omega \in \mathbb{R},$$

and similarly for $\hat{h}(\omega)$, $\hat{g}(\omega)$, etc., and $\widehat{M}^*(\omega)$ is the complex conjugate of $\widehat{M}(\omega)$.

The reconstruction is carried out by taking the reverse steps using the dual filters $\{\tilde{h}[k]\}$ and $\{\tilde{g}[k]\}$, which may be written as

$$\begin{pmatrix} \hat{c}_j(\omega) \\ \hat{c}_j(\omega+\pi) \end{pmatrix} = \widehat{\widetilde{M}}^T(\omega) \begin{pmatrix} \hat{c}_{j-1}(2\omega) \\ \hat{d}_{j-1}(2\omega) \end{pmatrix} \tag{2}$$

where $\widehat{\widetilde{M}}^T(\omega)$ is the transpose of the modulation matrix $\widehat{\widetilde{M}}(\omega)$ of the dual filters $\hat{\tilde{h}}(\omega)$ and $\hat{\tilde{g}}(\omega)$. Usually filters are devised to satisfy the perfect reconstruction condition

$$\widehat{\widetilde{M}}^T(\omega)\, \widehat{M}^*(\omega) = 2I, \tag{3}$$

which guarantees that the reconstructed signal is the same as the original signal, as it is clear from (1) and (2).

In the polyphase representation, we define the even and odd components

$$\hat{c}_{j,e}(\omega) = \sum_{k\in\mathbb{Z}} c_j[2k]\, e^{-i\omega k}, \quad \hat{c}_{j,o}(\omega) = \sum_{k\in\mathbb{Z}} c_j[2k+1]\, e^{-i\omega k}.$$

We then have the relation

$$\begin{pmatrix} \hat{c}_j(\omega) \\ \hat{c}_j(\omega+\pi) \end{pmatrix} = U(\omega) \begin{pmatrix} \hat{c}_{j,e}(2\omega) \\ \hat{c}_{j,o}(2\omega) \end{pmatrix}, \tag{4}$$

where

$$U(\omega) = \begin{pmatrix} 1 & e^{-i\omega} \\ 1 & e^{-i(\omega+\pi)} \end{pmatrix}.$$

Then, the decomposition (1) may be rewritten as

$$\begin{pmatrix} \hat{c}_{j-1}(2\omega) \\ \hat{d}_{j-1}(2\omega) \end{pmatrix} = \frac{1}{2}\widehat{M}^*(\omega)\, U(\omega) \begin{pmatrix} \hat{c}_{j,e}(2\omega) \\ \hat{c}_{j,o}(2\omega) \end{pmatrix} = \widehat{P}(2\omega)^\dagger \begin{pmatrix} \hat{c}_{j,e}(2\omega) \\ \hat{c}_{j,o}(2\omega) \end{pmatrix},$$

where $\widehat{P}(\omega)^\dagger$ is the Hermitian conjugate of the polyphase matrix

$$\widehat{P}(\omega) = \begin{pmatrix} \hat{h}_e(\omega) & \hat{g}_e(\omega) \\ \hat{h}_o(\omega) & \hat{g}_o(\omega) \end{pmatrix},$$

for which the perfect reconstruction (3) becomes

$$\widehat{\widetilde{P}}(\omega)\widehat{P}(\omega)^\dagger = I. \tag{5}$$

Thus, finding the perfect reconstuction filters amounts to find $\widehat{P}(\omega)$ and $\widehat{\widetilde{P}}(\omega)$ that satisfy (5). The simplest chioce is $\widehat{P}(\omega) = I$, which only splits up signals into even and odd-indexed samples, the so-called lazy transform.

A convenient strategy to construct the polyphase matrices is lifting. The odd-indexed sample $c_j[2k+1]$ is predicted by the predictor p of even-indexed samples $c_j[2k]$, and $c_j[2k+1]$ is replaced by $d_{j-1}[k]$ which is the difference between the original value and the prediction,

$$c_j[2k+1] \to d_{j-1}[k] = c_j[2k+1] - p(c_j[2k]).$$

Then, the even-indexed samples $c_j[2k]$ are updated by

$$c_j[2k] \to c_{j-1}[k] = c_j[2k] + u(d_{j-1}[k]),$$

where the normalization of the updater u is chosen such that the sum of the coarse components is halved by the decomposition,

$$\sum_k c_{j-1}[k] = \frac{1}{2}\sum_k c_j[k].$$

Finally, $c_j[k]$ and $d_j[k]$ are rescaled by $\sqrt{2}$ and $1/\sqrt{2}$, respectively, such that the total energy of the signal is preserved by the decomposition.

In the polyphase representation, lifting is to specify the predictor $\hat{p}(\omega)$ and the updater $\hat{u}(\omega)$ in the polyphase matrix as

$$\widehat{P}(\omega)^\dagger = \begin{pmatrix} \sqrt{2} & 0 \\ 0 & 1/\sqrt{2} \end{pmatrix} \begin{pmatrix} 1 & \hat{u}(\omega) \\ 0 & 1 \end{pmatrix} \begin{pmatrix} 1 & 0 \\ -\hat{p}(\omega) & 1 \end{pmatrix}, \tag{6}$$

where $\hat{p}(\omega)$ is defined by $\sum_k p(c_j[2k])e^{-i\omega k} = \hat{p}(\omega)\,\hat{c}_{j,e}(\omega)$, etc. The modulation matrix is then given by

$$\begin{pmatrix} \hat{h}^*(\omega) & \hat{h}^*(\omega+\pi) \\ \hat{g}^*(\omega) & \hat{g}^*(\omega+\pi) \end{pmatrix} = \widehat{M}^*(\omega) = \widehat{P}(2\omega)^\dagger U(\omega)^{-1}.$$

We choose the dual polyphase matrix $\widehat{\widetilde{P}}(\omega) = \widehat{P}(\omega)^{\dagger\,-1}$, which guarantees the perfect reconstruction (5). The dual filters may be found from $\widehat{\widetilde{M}}^T(\omega) = U(\omega)\,\widehat{\widetilde{P}}(2\omega)$.

For example, the choice $\hat{p}(\omega) = 1$ and $\hat{u}(\omega) = 1/2$ gives Haar filter, $\hat{h}(\omega) = \hat{\tilde{h}}(\omega) = (1+e^{-i\omega})/\sqrt{2}$, and $\hat{g}(\omega) = \hat{\tilde{g}}(\omega) = (-1+e^{-i\omega})/\sqrt{2}$, which turns out to be orthogonal. On the other hand, if we choose the linear prediction,

$$\hat{p}(\omega) = \frac{1+e^{i\omega}}{2}, \quad \hat{u}(\omega) = \frac{1+e^{-i\omega}}{4},$$

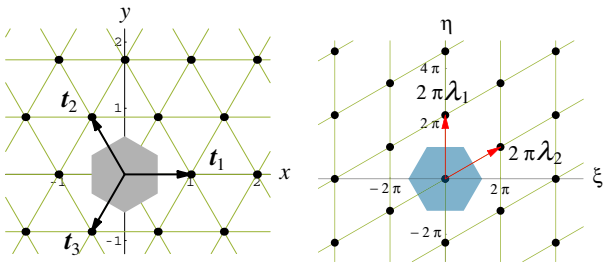

Figure 1: The primitive translation vectors, Bravais lattice, and the Wigner-Seitz cell (left), the reciprocal lattice vectors, reciprocal lattice, and the Brilloin zone (right)

then we find the CDF (2,2) filter [9]

$$\begin{aligned} \hat{h}(\omega) &= \frac{-e^{i2\omega} + 2e^{i\omega} + 6 + 2e^{-i\omega} - e^{-i2\omega}}{4\sqrt{2}} \\ \hat{g}(\omega) &= \frac{-1 + 2e^{-i\omega} - e^{-i2\omega}}{2\sqrt{2}}. \end{aligned} \tag{7}$$

which we call the linear prediction filter. We wish to follow the same method for the construction of our triangular wavelets in the next section.

3. TRIANGULAR BIORTHOGONAL WAVELETS

Discrete signals are naturally indexed by integers in one-dimension, but the indexing may become a nontrivial problem in dimensions more than one. We find it convenient to employ the primitive translation vectors [10], which is used In solid state physics in classifying crystal structures.

In two-dimensional plane, we define two primitive translation vectors

$$\boldsymbol{t}_1 = \begin{pmatrix} 1 & 0 \end{pmatrix}^T, \quad \boldsymbol{t}_2 = \begin{pmatrix} -\frac{1}{2} & \frac{\sqrt{3}}{2} \end{pmatrix}^T.$$

It is convenient also to define $\boldsymbol{t}_3 = -\boldsymbol{t}_1 - \boldsymbol{t}_2$ and $\boldsymbol{t}_0 = \boldsymbol{0}$. The regular traiangular Baivais lattice is defined by

$$\Lambda = \{\boldsymbol{t} = n_1\boldsymbol{t}_1 + n_2\boldsymbol{t}_2 | \, (n_1, n_2) \in \mathbb{Z}^2\}.$$

The domain containing all the points whose closest site is a given site $\boldsymbol{t} \in \Lambda$ is the Wigner-Seitz cell of the site. In our regular triangular lattice Λ, the Wigner-Seitz cell is a hexagon, which plays the role of a pixel of an image. The vectors $\boldsymbol{t}_m$, $m = 1, 2, 3$, the Bravais lattice Λ, and the Wigner-Seitz cell are shown in Figure 1 (left).

The reciplocal lattice vectors are defined by

$$\boldsymbol{\lambda}_1 = \begin{pmatrix} 0 & \frac{2}{\sqrt{3}} \end{pmatrix}^T, \quad \boldsymbol{\lambda}_2 = \begin{pmatrix} 1 & \frac{1}{\sqrt{3}} \end{pmatrix}^T,$$

and $\boldsymbol{\lambda}_3 = \boldsymbol{\lambda}_1 + \boldsymbol{\lambda}_2$. They generate the reciplocal lattice

$$\widehat{\Lambda} = \{2\pi(\boldsymbol{\lambda} = m_1\boldsymbol{\lambda}_1 + m_2\boldsymbol{\lambda}_2) | \, (m_1, m_2) \in \mathbb{Z}^2\}.$$

The Wigner-Seitz cell of the reciprocal lattice $\widehat{\Lambda}$ is the Brilloin zone. The vectors $2\pi\boldsymbol{\lambda}_m$, $m = 1, 2$, the reciplocal lattice $\widehat{\Lambda}$, and the Brilloin zone are shown in Figure 1 (right).

The LP filter $\{h[\boldsymbol{t}]\}_{\boldsymbol{t}\in\Lambda}$ is now defined on the Bravais lattice Λ, and

$$\hat{h}(\boldsymbol{\omega}) = \sum_{\boldsymbol{t}\in\Lambda} h[\boldsymbol{t}]\, e^{-i\boldsymbol{\omega}\cdot\boldsymbol{t}}, \quad \boldsymbol{\omega} \in \mathbb{R}^2.$$

Since $\hat{h}(\omega)$ is periodic with respect to the translation $\omega \to \omega + 2\pi\boldsymbol{\lambda}$, the Brilloin zone is its defining domain. A crucial observation is that all the sites of Λ may be classified into four independent sublattices

$$\Lambda_m = \{2\boldsymbol{t} + \boldsymbol{t}_m | \, \boldsymbol{t} \in \Lambda\}, \quad m = 0, 1, 2, 3,$$

which play the role of even and odd indices in one dimension. Accordingly, the filter may be represented as the sum of the corresponding components

$$\hat{h}_m(\omega) = \sum_{t \in \Lambda} h[2\boldsymbol{t} + \boldsymbol{t}_m] e^{-i\omega\cdot\boldsymbol{t}}, \quad m = 0, 1, 2, 3,$$

as

$$\begin{pmatrix} \hat{h}(\omega) \\ \hat{h}(\omega + \pi\boldsymbol{\lambda}_1) \\ \hat{h}(\omega + \pi\boldsymbol{\lambda}_2) \\ \hat{h}(\omega + \pi\boldsymbol{\lambda}_3) \end{pmatrix} = U(\omega) \begin{pmatrix} \hat{h}_0(2\omega) \\ \hat{h}_1(2\omega) \\ \hat{h}_2(2\omega) \\ \hat{h}_1(2\omega) \end{pmatrix}$$

where

$$U(\omega) = \begin{pmatrix} 1 & e^{-i\omega\cdot\boldsymbol{t}_1} & e^{-i\omega\cdot\boldsymbol{t}_2} & e^{-i\omega\cdot\boldsymbol{t}_3} \\ 1 & e^{-i\omega\cdot\boldsymbol{t}_1} & -e^{-i\omega\cdot\boldsymbol{t}_2} & -e^{-i\omega\cdot\boldsymbol{t}_3} \\ 1 & -e^{-i\omega\cdot\boldsymbol{t}_1} & e^{-i\omega\cdot\boldsymbol{t}_2} & -e^{-i\omega\cdot\boldsymbol{t}_3} \\ 1 & -e^{-i\omega\cdot\boldsymbol{t}_1} & -e^{-i\omega\cdot\boldsymbol{t}_2} & e^{-i\omega\cdot\boldsymbol{t}_3} \end{pmatrix}.$$

It is a straightforward generalization of (4).

We now extend the lifting (6) to two dimensions, and define the polyphase matrices in the form

$$\widehat{P}(\omega)^\dagger = \begin{pmatrix} 2 & 0 & 0 & 0 \\ 0 & \frac{1}{2} & 0 & 0 \\ 0 & 0 & \frac{1}{2} & 0 \\ 0 & 0 & 0 & \frac{1}{2} \end{pmatrix} \begin{pmatrix} 1 & \hat{u}_1 & \hat{u}_2 & \hat{u}_3 \\ 0 & 1 & 0 & 0 \\ 0 & 0 & 1 & 0 \\ 0 & 0 & 0 & 1 \end{pmatrix} \begin{pmatrix} 1 & 0 & 0 & 0 \\ -\hat{p}_1 & 1 & 0 & 0 \\ -\hat{p}_2 & 0 & 1 & 0 \\ -\hat{p}_3 & 0 & 0 & 1 \end{pmatrix}, \tag{8}$$

with the predictors $\hat{p}_m(\omega)$ and the updaters $\hat{u}_m(\omega)$, and $\widehat{\widetilde{P}}(\omega) = \widehat{P}(\omega)^{\dagger^{-1}}$.

The four polyphase components are decomposed by the polyphase matrix as

$$\begin{pmatrix} \hat{c}_{j-1}(\omega) \\ \hat{d}_{1,j-1}(\omega) \\ \hat{d}_{2,j-1}(\omega) \\ \hat{d}_{3,j-1}(\omega) \end{pmatrix} = \widehat{P}^\dagger(\omega) \begin{pmatrix} \hat{c}_{0,j}(\omega) \\ \hat{c}_{1,j}(\omega) \\ \hat{c}_{2,j}(\omega) \\ \hat{c}_{4,j}(\omega) \end{pmatrix}.$$

We remark that there are three detail components $\hat{d}_{m,j-1}(\omega)$, $m = 1, 2, 3$, whereas the data is decomposed into LL, LH, HL, and HH (L= coarse, H= detail) components in the usual tensor product transform. The modulation matrices are

$$\begin{pmatrix} \hat{h}^*(\omega) & \hat{h}^*(\omega + \pi\boldsymbol{\lambda}_1) & \hat{h}^*(\omega + \pi\boldsymbol{\lambda}_2) & \hat{h}^*(\omega + \pi\boldsymbol{\lambda}_3) \\ \hat{g}_1^*(\omega) & \hat{g}_1^*(\omega + \pi\boldsymbol{\lambda}_1) & \hat{g}_1^*(\omega + \pi\boldsymbol{\lambda}_2) & \hat{g}_1^*(\omega + \pi\boldsymbol{\lambda}_3) \\ \hat{g}_2^*(\omega) & \hat{g}_2^*(\omega + \pi\boldsymbol{\lambda}_1) & \hat{g}_2^*(\omega + \pi\boldsymbol{\lambda}_2) & \hat{g}_2^*(\omega + \pi\boldsymbol{\lambda}_3) \\ \hat{g}_3^*(\omega) & \hat{g}_3^*(\omega + \pi\boldsymbol{\lambda}_1) & \hat{g}_3^*(\omega + \pi\boldsymbol{\lambda}_2) & \hat{g}_3^*(\omega + \pi\boldsymbol{\lambda}_3) \end{pmatrix}$$

$$= \widehat{M}^*(\omega) = \widehat{P}(2\omega)^\dagger U(\omega)^\dagger,$$

and $\widehat{\widetilde{M}}^T(\omega) = U(\omega)\,\widehat{\widetilde{P}}(2\omega)$. The perfect reconstruction condition $\widehat{\widetilde{P}}(2\omega)\,\widehat{P}(2\omega)^\dagger = I$, i.e.,

$$\widehat{\widetilde{M}}^T(\omega)\,\widehat{M}^*(\omega) = 4I$$

will be guaranteed by construction. In particular, the equality

$$\hat{\tilde{h}}(\omega)\,\hat{h}^*(\omega) + \sum_{m=1}^{3} \hat{\tilde{g}}_m(\omega)\,\hat{g}_m^*(\omega) = 4 \tag{9}$$

implies the halfband condition.

Once the filters are found, the two-dimensional scaling functions $\phi(\boldsymbol{r})$ and wavelets $\psi_m(\boldsymbol{r})$, $m = 1, 2, 3$, $\boldsymbol{r} \in \mathbb{R}^2$, are defined by their Fourier transform,

$$\hat{\phi}(\omega) = \prod_{j=1}^{\infty} \frac{1}{2}\hat{h}\Big(\frac{\omega}{2^j}\Big), \quad \hat{\psi}_m(\omega) = \frac{1}{2}\hat{g}_m\Big(\frac{\omega}{2}\Big)\hat{\phi}\Big(\frac{\omega}{2}\Big), \quad \omega \in \mathbb{R}^2.$$

We do not further consider these functions, and concentrate on the properties of the filters. We now proceed to some examples.

3.1 Biorthogonal Triangular Haar

The simplest choise is

$$\hat{p}_m(2\omega) = 1, \quad \hat{u}_m(2\omega) = \frac{1}{4}.$$

Then we find the filters

$$\begin{pmatrix} \hat{h}(\omega) \\ \hat{g}_1(\omega) \\ \hat{g}_2(\omega) \\ \hat{g}_3(\omega) \end{pmatrix} = \frac{1}{2} \begin{pmatrix} 1 & 1 & 1 & 1 \\ -1 & 1 & 0 & 0 \\ -1 & 0 & 1 & 0 \\ -1 & 0 & 0 & 1 \end{pmatrix} \begin{pmatrix} 1 \\ e^{-i\omega\cdot\boldsymbol{t}_1} \\ e^{-i\omega\cdot\boldsymbol{t}_2} \\ e^{-i\omega\cdot\boldsymbol{t}_3} \end{pmatrix},$$

$$\begin{pmatrix} \hat{\tilde{h}}(\omega) \\ \hat{\tilde{g}}_1(\omega) \\ \hat{\tilde{g}}_2(\omega) \\ \hat{\tilde{g}}_3(\omega) \end{pmatrix} = \frac{1}{2} \begin{pmatrix} 1 & 1 & 1 & 1 \\ -1 & 3 & -1 & -1 \\ -1 & -1 & 3 & -1 \\ -1 & -1 & -1 & 3 \end{pmatrix} \begin{pmatrix} 1 \\ e^{-i\omega\cdot\boldsymbol{t}_1} \\ e^{-i\omega\cdot\boldsymbol{t}_2} \\ e^{-i\omega\cdot\boldsymbol{t}_3} \end{pmatrix}.$$

The LP filters are the same as the orthogonal triangular haar, discussed previously [12], and we do not discuss this case further here.

3.2 Triangular Linear Prediction Filter

If we choose

$$\hat{p}_m(2\omega) = \frac{1 + e^{i2\omega\cdot\boldsymbol{t}_m}}{2}, \quad \hat{u}_m(2\omega) = \frac{1 + e^{-i2\omega\cdot\boldsymbol{t}_m}}{8}, \tag{10}$$

we have the triangular version of (7). We display the filter coefficients and the Fourier transform in Figure 2–5. The filters $\hat{g}_m(\omega)$, $m = 1$ and 3 are simply $2\pi/3$ rotations of the $m = 2$ case. Figure 6 shows the frequency response of the LP filter

$$\hat{\tilde{h}}(\omega\boldsymbol{\lambda}_m)\,\hat{h}^*(\omega\boldsymbol{\lambda}_m) = 2 + \frac{9}{4}\cos\omega - \frac{1}{4}\cos 3\omega$$

in the $\boldsymbol{\lambda}_m$, $m = 1, 2, 3$ direction, Note that at the alias point,

$$\hat{\tilde{h}}(\omega\boldsymbol{\lambda}_m)\,\hat{h}^*(\omega\boldsymbol{\lambda}_m) \propto (\omega - \pi)^4,$$

which is higher order compared with the Haar filter.

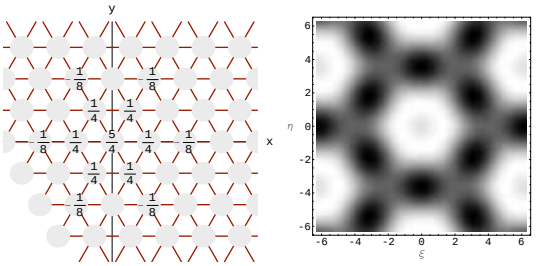

Figure 2: The linear prediction LP filter coefficients $h[\boldsymbol{t}]$ and $|\hat{h}(\boldsymbol{\omega})|$

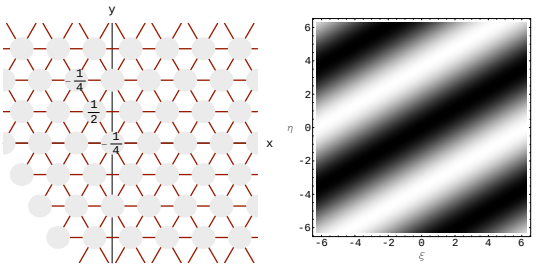

Figure 3: The linear prediction HP filter coefficients $g_2[\boldsymbol{t}]$ and $|\hat{g}_2(\boldsymbol{\omega})|$

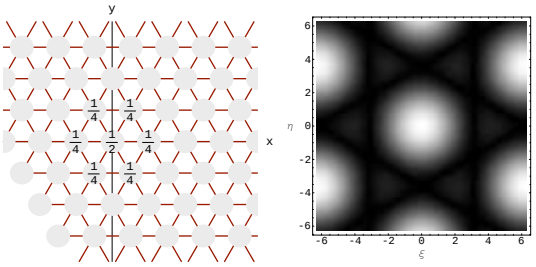

Figure 4: The linear prediction dual filter coefficients $\tilde{h}[\boldsymbol{t}]$ and $|\hat{\tilde{h}}(\boldsymbol{\omega})|$

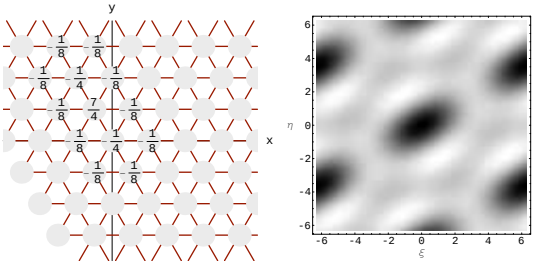

Figure 5: The linear prediction dual filter coefficients $\tilde{g}_2[\boldsymbol{t}]$ and $|\hat{\tilde{g}}_2(\boldsymbol{\omega})|$

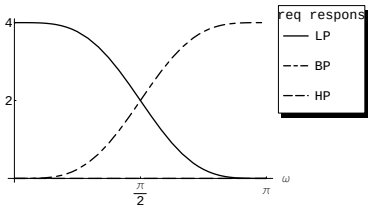

Figure 6: The frequency response of linear filters

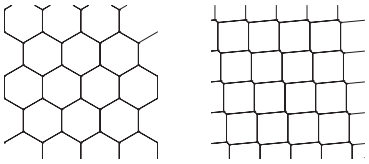

Figure 7: The honeycomb and nearly square array of Wigner-Seitz cells

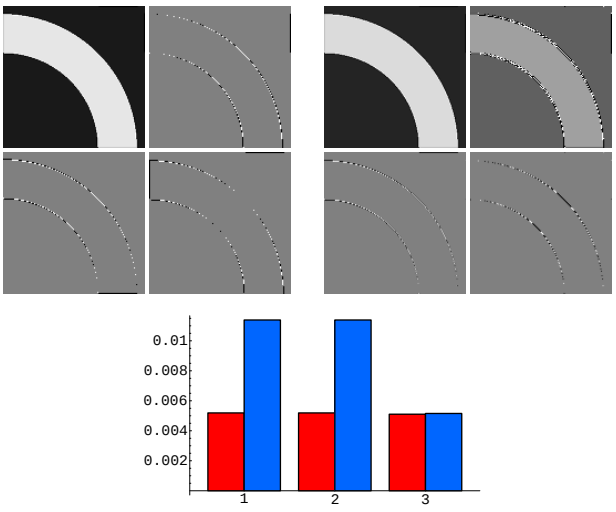

Figure 8: Images and $\sum_{\boldsymbol{t}} |d_{m,j-1}[\boldsymbol{t}]|$ of a white circle, TriDWT (left) and TensorDWT (right)

4. APPLICATIONS TO IMAGE PROCESSING

Our triangular filters are formally designed to deal with two dimensional data defined on the regular triangular Bravais lattice, whereas image data are usually rectangular arrays of numbers. Nothing prevents us to adhere to regular triangles, however. In fact, we may rotate the second primitive translation vector $\boldsymbol{t}_2$ clockwise to approach the y axis. In this case, the Wigner-Seitz cell will be deformed to form nearly rectangular arrays, as shown in Figure 7. We treat image data as the original image $\{c_j[\boldsymbol{t}]\}$, and decomposed images $\{c_{j-1}[\boldsymbol{t}]\}$, and $\{d_{j-1}[\boldsymbol{t}]\}$, $\boldsymbol{t} \in \Lambda$, in this limit. We compare the decomposition of sample images by triangular linear prediction filter (TriDWT), and the tensor product wavelet transform (TensorDWT) below. We see that the values $\{d_{j-1}[\boldsymbol{t}]\}$ are evenly distributed in TriDWT, whereare in the usual TensorDWT the HH component does not contain much energy. This implies that the isotropy of images is well respected.

Figure 8 (upper left) shows the TriDWT decomposition of a white circle on black background, the coarse c, and detail d_1, d_2, d_3 components, in the order from top to bottom, and left to right. Figure 8 (upper right) shows the corresponding TensorDWT decomposition, the coarse LL and detail LH, LH, HH components, and the absolute values $\sum_{\boldsymbol{t}\in\Lambda_0} |c_{j-1}[\boldsymbol{t}]|$ and $\sum_{\boldsymbol{t}\in\Lambda_m} |d_{m,j-1}[\boldsymbol{t}]|$, $m = 1, 2, 3$, are plotted in the bottom of the figure.

In actual images, such as a finger pring in Figure 9–10, similar features are observed, except for some directionality exist that are properties of individual images. In particular, it is clear that energy contained in the HH components of "Barbara" is much less in TensorDWT as compared with d_3

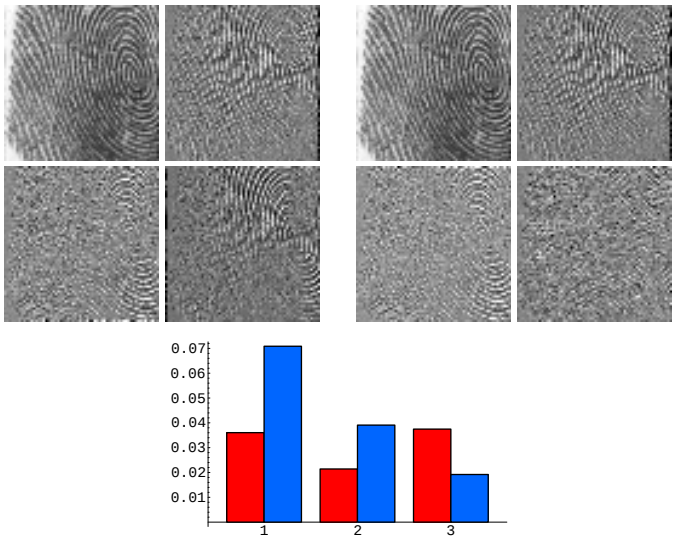

Figure 9: Images and $\sum_{\boldsymbol{t}} |d_{m,j-1}[\boldsymbol{t}]|$ of a finger pring, TriDWT (left) and TensorDWT (right)

of TriDWT.

5. CONCLUSION AND FURTHER STUDIES

We constructed non-separable biorthogonal wavelet filters defined on the regular triangular lattice. In particular, features of the filters resulted from linear prediction are applied to sample images. As expected, the energy (here, L^1 norm, pricisely) is more evenly distributed in the three detail components as compared with less energy in the HH component in the tensor product wavelet transform. In this sense, our triangular wavelets look promising in preserving isotropy of images. Note that the filter coefficients are all integral multiples of powers of two, and the transform can easily be carried out by lifting, so that they are advantageous in computer implementation.

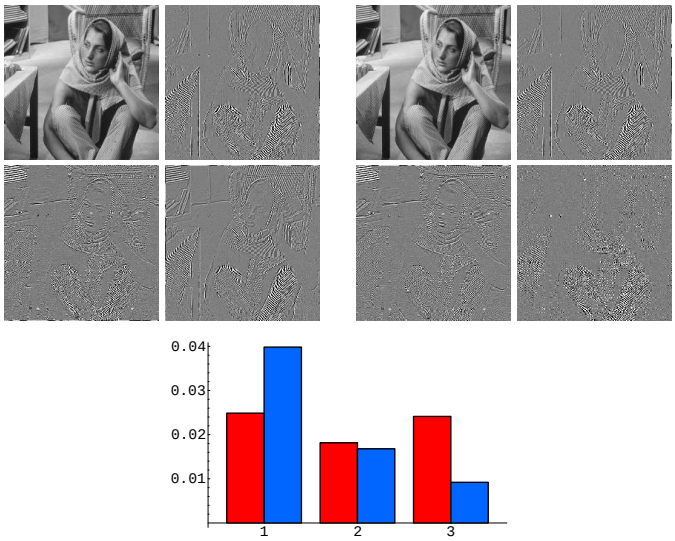

Figure 10: Images and $\sum_{\boldsymbol{t}} |d_{m,j-1}[\boldsymbol{t}]|$ of "Barbara", TriDWT (left) and TensorDWT (right)

We finally remark that the polyphase matrix (8) may be modifed as

$$\widehat{P^{\dagger}}(\omega) \to \widehat{P^{\dagger}}(\omega) \begin{pmatrix} 1 & 0 & 0 & 0 \\ 0 & -1 & 1 & 1 \\ 0 & 1 & -1 & 1 \\ 0 & 1 & 1 & -1 \end{pmatrix}.$$

In this case, the orthogonal Haar filter will emergy, while the linear prediction filter will be modified. In any case, more samples as well as variations of triangular filters including such cases deserve further study.

REFERENCES

[1] S. Mallat, *A wavelet tour of signal processing*, 2nd ed., Academic Press, 2001

[2] J. Kovačević and M. Vetterli, "Nonseparable multidimensional perfect reconstruction filter banks and wavelet bases for $\mathbb{R}^n$," *IEEE Trans. Information Theory*, vol.38(2), 533–555, 1992.

[3] N. Kingsbury, "The dual-tree complex wavelet transform: a new technique for shift invariance and directional filters," *Proc. 8th IEEE DSP Workshop*, paper no.86, 1998.

[4] H. Kawabata, H. Toda, Z. Zhang, and H. Fujiwara, "A new complex wavelet transform by using RI-spline wavelet," in *Proc. IEEE Int. Conf. Acoust., Speech, Signal Processing*, Montreal, May 2004, vol.2, pp.937–940.

[5] W. Sweldens, "The lifting scheme: a custom-design construction of biorthogonal wavelets," *Applied and Computational Harmonic Analysis*, vol. 3(2), pp. 186–200, 1996.

[6] W. Sweldens, "The lifting scheme: A Construction of second generation wavelets," *SIAM J. Math. Anal.*, 29(2), 511–546, 1997.

[7] P. Schröder and W. Sweldens, "Sperical wavlets: efficiently representing functions on the sphere," *Computer Graphics Proceedings (SIGGRAPH 95)*, 161–172, 1995.

[8] I. Daubechies, I. Guskov, P. Schröder, and W.Sweldens, "Wavelets on Irregular Point Sets," *Phil. Trans. R.Soc.Lon.A.*, vol.357(1760), 2397–2413, 2000.

[9] A. Cohen, I. Daubechies, and J. Feauveau, "Biorthogonal Bases of Compactly supported Wavelets," *Comm. Pure Appl. Math.*, vol.45, 486–560, 1992.

[10] G. Grosso and G. P. Parravicini, *Solid State Physics*, Elsevier Academic Press, 2000.

[11] S. Sakakibara, "Aspects of Wavelet Analysis," *Proceedings of Sice2005, International Conference on Instrumentation, Control and Information Technology*, Okayama University, Okayama, Japan, August 8–10, paper no. MP1-03-5, 2005.

[12] K. Fujinoki and S. Sakakibara, "Triangular Wavelet Basis and its Application," *Proceedings of Sice2005, International Conference on Instrumentation, Control and Information Technology*, Okayama University, Okayama, Japan, August 8–10, paper no. MP1-03-4, 2005.